nature chemical biology

ARTICLE

PUBLISHED ONLINE: 8 MAY 2017 | DOI: 10.1038/NCHEMBIO.2376

Plasticity, dynamics, and inhibition of emerging tetracycline resistance enzymes

Jooyoung Park[1,7], Andrew J Gasparrini[2,7], Margaret R Reck[3], Chanez T Symister[3], Jennifer L Elliott[1], Joseph P Vogel[1], Timothy A Wencewicz[3,8*], Gautam Dantas[1,2,4,5,8*] & Niraj H Tolia[1,6,8*]

Although tetracyclines are an important class of antibiotics for use in agriculture and the clinic, their efficacy is threatened by increasing resistance. Resistance to tetracyclines can occur through efflux, ribosomal protection, or enzymatic inactivation. Surprisingly, tetracycline enzymatic inactivation has remained largely unexplored, despite providing the distinct advantage of antibiotic clearance. The tetracycline destructases are a recently discovered family of tetracycline-inactivating flavoenzymes from pathogens and soil metagenomes that have a high potential for broad dissemination. Here, we show that tetracycline destructases accommodate tetracycline-class antibiotics in diverse and novel orientations for catalysis, and antibiotic binding drives unprecedented structural dynamics facilitating tetracycline inactivation. We identify a key inhibitor binding mode that locks the flavin adenine dinucleotide cofactor in an inactive state, functionally rescuing tetracycline activity. Our results reveal the potential of a new tetracycline and tetracycline destructase inhibitor combination therapy strategy to overcome resistance by enzymatic inactivation and restore the use of an important class of antibiotics.

Antibiotics revolutionized the treatment of infectious diseases, enabling substantial reductions in deaths caused by infection over the past 80 years. However, the prolific anthropogenic use of these life-saving chemotherapeutics in the clinic and in agriculture has also selected for a steady increase in antibiotic resistance in both benign and pathogenic bacteria[1]. Regrettably, increasing antibiotic resistance has been accompanied by a decrease in the development and regulatory approval of new antibiotics[2], threatening the end of the modern antibiotic era. The likely origin of virtually all clinical antibiotic resistance genes are environmental microbial communities, which harbor ancient and diverse resistomes[3–9]. Indeed, environmental reservoirs have been identified for a number of recently emerged and rapidly disseminating resistance genes representing urgent clinical threats (for example, plasmid-borne and chromosomally acquired carbapenem[10], colistin[11], and quinolone[12] resistance genes). This motivates the need to better understand resistance mechanisms of environmental origin before they become widespread in the clinic, and this will ultimately guide new drug discovery and therapeutic strategies that mitigate emerging mechanisms of resistance.

Despite growing resistance, the tetracyclines remain among the most widely used antibiotics in clinical and agricultural settings[13]. Indeed, tetracyclines ranked in the top three antibiotics both in clinical prescriptions in the United States in 2010 (representing 15% of all antibiotic prescriptions) and in global sales for animal use in 2009 ($500 million in sales)[14]. Furthermore, next-generation derivatives are currently fueling a tetracycline renaissance, with the 2005 clinical approval of tigecycline[15] and ongoing late-stage clinical trials of eravacycline and omadacycline[16,17] justifying urgent interrogation of emerging and novel tetracycline resistance mechanisms. Previously, tetracycline resistance was thought to occur almost exclusively by two mechanisms: ribosomal protection or antibiotic efflux[13,18]. However, an alternate mechanism—enzymatic inactivation—has been documented in benign and pathogenic bacteria, such as the enzyme Tet(X)[19–27]. We recently identified a new family of tetracycline-inactivating enzymes through functional metagenomic selections for tetracycline resistance from 18 grassland and agricultural soils[9]. We showed that these nine proteins, Tet(47)–Tet(55), were able to enzymatically inactivate tetracycline, resulting in 16- to 64-fold increases in minimum inhibitory concentrations (MICs)[28] when expressed in *Escherichia coli*.

Here, we pursued a multipronged structural, *in vitro* enzymatic, and bacterial phenotypic investigation of the emerging tetracycline destructases. We show that a recently identified tetracycline destructase confers tetracycline resistance to a known soil-derived human pathogen. We hypothesized that structural characteristics of tetracycline-inactivating enzymes would reveal useful information about their unique activity profiles and lead to the rational design of inhibitors, in a process similar to the development of the widely employed β-lactamase inhibitors[29]. Discerning the structural and mechanistic details of conformational or transitional states in target proteins has been crucial for the rational design of successful inhibitors in a number of cases, as exemplified by inhibitors of HIV-1 protease[30] and mechanistic inhibitors of glycosyltransferases that involve considerable conformational movement in the active site[31]. Through structure–function analyses of four tetracycline destructases alone and in complex with tetracycline-class ligands, we present the molecular basis for unexpected structural dynamics in tetracycline destructases driven by antibiotic binding. These unprecedented changes provide a novel mechanism for inhibition that has the potential to synergistically restore tetracycline activity and rescue an important class of antibiotics.

RESULTS

Tetracycline inactivation by *Legionella longbeachae*

The tetracycline destructase family was initially discovered by functional metagenomic selection for tetracycline resistance from

[1]Department of Molecular Microbiology, Washington University School of Medicine, St. Louis, Missouri, USA. [2]Center for Genome Sciences and Systems Biology, Washington University School of Medicine, St. Louis, Missouri, USA. [3]Department of Chemistry, Washington University in St. Louis, St. Louis, Missouri, USA. [4]Department of Pathology and Immunology, Washington University School of Medicine, St. Louis, Missouri, USA. [5]Department of Biomedical Engineering, Washington University in St. Louis, St. Louis, Missouri, USA. [6]Department of Biochemistry and Molecular Biophysics, Washington University School of Medicine, St. Louis, Missouri, USA. [7]These authors contributed equally to this work. [8]These authors jointly directed this work. *e-mail: tolia@wustl.edu, dantas@wustl.edu or wencewicz@wustl.edu

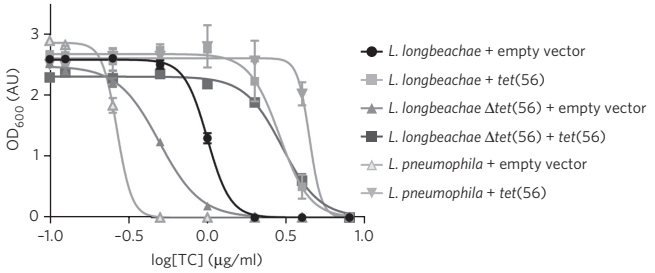

Figure 1 | Dose–response curve showing the effect of tetracycline on growth of *Legionella* strains. Deletion of *tet*(56) from *L. longbeachae* causes an increase in tetracycline (TC) sensitivity. Complementation with a plasmid containing the *tet*(56) insert rescues the tetracycline resistance phenotype, compared to strains bearing the empty vector control. Furthermore, introduction of the complementing vector into *L. pneumophila*, which lacks a *tet*(56) homolog, results in an increase in tetracycline resistance. Data are represented as mean ± s.d. of three technical replicates. OD_{600}, optical density at 600 nm; AU, absorbance units.

soil samples[9]. We also observed a homolog of the tetracycline destructase genes, termed *tet*(56), in the soil-derived human pathogen *Legionella longbeachae*, a causative agent of Pontiac fever and Legionnaires' disease[32,33]. Like the other tetracycline destructases, Tet(56) is able to inactivate tetracycline *in vitro*, and expression of *tet*(56) in *E. coli* confers high-level tetracycline resistance[28]. To confirm that *tet*(56) is a functional resistance determinant in *L. longbeachae*, we deleted the gene and examined the strain for changes in drug sensitivity. Deletion of the chromosomally encoded *tet*(56) resulted in an increase in tetracycline sensitivity to *L. longbeachae* (**Fig. 1**). Moreover, overexpression of *tet*(56) in the *L. longbeachae* Δ*tet*(56) strain resulted in increased tetracycline resistance to levels even higher than those seen for the wild-type *L. longbeachae* strain containing empty vector. Finally, expression of *tet*(56) in *Legionella pneumophila*, which lacks a tetracycline destructase homolog, also dramatically increased the tetracycline resistance of the strain. These results demonstrate that tetracycline destructases are already functional in a known human pathogen, and that their introduction into a related pathogen would lead to increased antibiotic resistance.

Structural architecture and dynamics of Tet(50), Tet(51), Tet(55), and Tet(56)

We began our structural analysis by solving the X-ray crystal structures of four tetracycline-inactivating enzymes: Tet(50), Tet(51), Tet(55), and Tet(56) (**Fig. 2a** and **Supplementary Results, Supplementary Fig. 1a–e**). Despite only sharing ~24% amino acid identity with the previously crystallized Tet(X) and requiring initial structure determination via experimental phasing (**Supplementary Table 1**), Tet(50,51,55,56) and Tet(X) exhibit a similar overall architecture. Each possesses a flavin adenine dinucleotide (FAD)-binding Rossmann-type fold domain, a tetracycline-binding domain, and a C-terminal α-helix that bridges the two domains (**Fig. 2a**). Surprisingly, each of the new structures revealed an unexpected second α-helix at the C terminus (**Fig. 2a–c**) that is not present in Tet(X) (**Fig. 2d**) and could not be predicted on the basis of their primary sequences. Comparisons to co-crystal structures of Tet(X) in complex with either chlortetracycline (PDB ID: 2Y6R) or iodtetracycline (PDB ID: 2Y6Q)[27] reveal that this helical extension comes in close proximity to the tetracycline-binding site (**Fig. 2d**), contributing to the formation of a substrate-loading channel. In the Tet(50) crystal structure, we observed two distinct monomers in the asymmetric unit. In Tet(50) monomer A, this substrate-loading channel is blocked by a flexible loop (**Fig. 2b,e**), whereas in Tet(50) monomer B, the channel is open, allowing tetracycline to access the substrate-binding site (**Fig. 2c,f**). The absence of the second α-helix

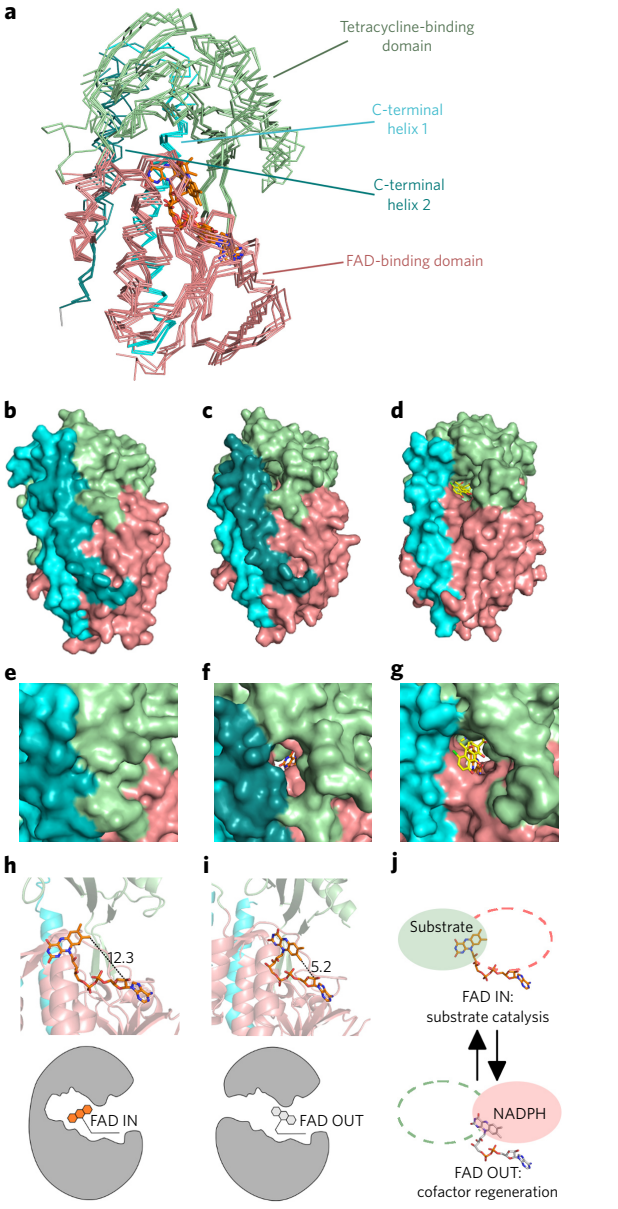

Figure 2 | Crystal structures of Tet(50), Tet(51), Tet(55), and Tet(56) reveal a conserved architecture, structural changes that enable substrate-loading channel accessibility, and two conformations of the FAD cofactor. (**a**) Overlay of the Tet(50) monomer A, Tet(50) monomer B, Tet(51), Tet(55), and Tet(56) crystal structures. The FAD-binding domain (salmon), the tetracycline-binding domain (pale green), the first (cyan) and second (deep teal) C-terminal α-helixes, and FAD molecules (orange) are shown. (**b–d**) Surface representation of Tet(50) monomer A with the substrate-loading channel closed (**b**), Tet(50) monomer B with the substrate-loading channel open (**c**), and a previously published structure of Tet(X) with chlortetracycline (yellow) bound—PDB ID 2Y6R (**d**). (**e–g**) Zoomed-in view of the closed substrate-loading channel in Tet(50) monomer A (**e**), the open substrate-loading channel in Tet(50) monomer B (**f**), and the wide-open substrate-binding site in Tet(X) (**g**). (**h**) The FAD cofactor adopts the IN conformation in Tet(50) monomer A, characterized by a 12.3-Å distance between the C8M and C2B atoms of the FAD molecule. (**i**) The FAD cofactor adopts the OUT conformation in Tet(50) monomer B, characterized by a 5.2-Å distance between the C8M and C2B atoms of the FAD molecule. (**j**) The IN conformation of FAD allows substrate catalysis. The OUT conformation of FAD allows regeneration of the reduced FAD for the next round of catalysis. Green area, substrate-binding site; pink area, putative NADPH binding site.

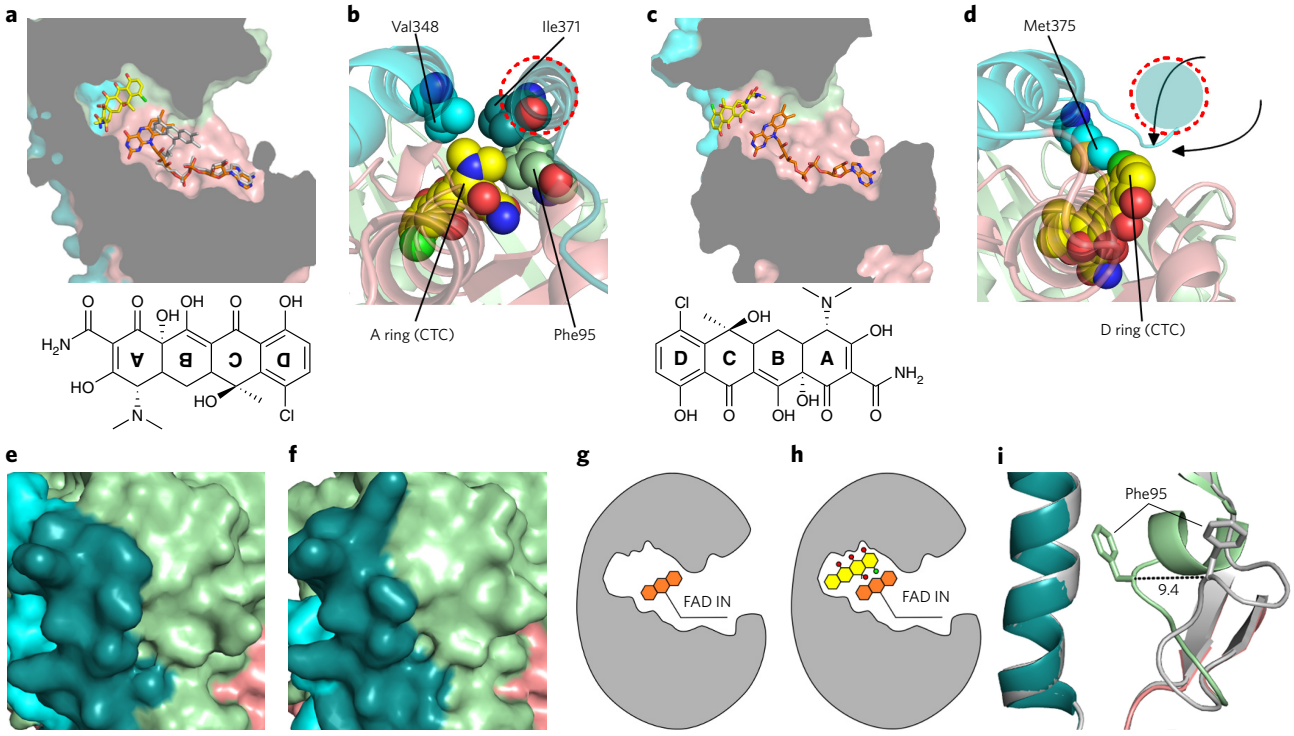

Figure 3 | Tet(50)–chlortetracycline structure reveals an unexpected mode of binding that drives substrate-loading channel closure and FAD conversion. (**a**) Chlortetracycline (CTC) binds to Tet(50) in a ~180° rotated orientation relative to Tet(X)–chlortetracycline, with FAD in the IN conformation (orange); a model of FAD OUT (gray) is overlaid. (**b**) The rotated orientation in the Tet(50)–chlortetracycline structure is supported by van der Waals contacts from Val348 (cyan) and Ile371 (deep teal) of the two C-terminal α-helices in Tet(50) to the dimethylamine group of the A ring of chlortetracycline. Additionally, Phe95 from the flexible loop makes contacts with the dimethylamine group and closes off the substrate-binding site. (**c**) Chlortetracycline binds Tet(X) with the D ring distal to FAD. The substrate-binding site is widely exposed to bulk solvent. (**d**) Met375 from the first C-terminal α-helix in Tet(X) (cyan) makes van der Waals contacts to the D ring of chlortetracycline. A second C-terminal helix (red dashed circle, colored in deep teal) does not exist in Tet(X), and therefore substrate can potentially enter from various possible directions. (**e**) Surface representation of Tet(50)–chlortetracycline monomer A. (**f**) Surface representation of Tet(50)–chlortetracycline monomer B. (**g**) In Tet(50)–chlortetracycline monomer A, FAD is in the IN conformation, the loop is closed, and no chlortetracycline is bound. (**h**) In Tet(50)–chlortetracycline monomer B, FAD is in the IN conformation, the loop is closed, and chlortetracycline is bound. (**i**) Whereas the substrate-loading channel is open in Tet(50) monomer B, when FAD is OUT, in the absence of chlortetracycline (gray), the flexible loop containing Phe95 closes over the channel in Tet(50)–chlortetracycline monomer B, and FAD now becomes IN.

in Tet(X) results in a widely exposed entrance to the substrate-binding site (**Fig. 2d**,**g**), which likely contributes to alternate substrate specificity of this enzyme.

FAD conformation modulates substrate-loading channel

Tetracycline destructases are flavoenzymes that utilize an FAD cofactor to degrade their substrate[34,35]. These enzymes bind FAD in two distinct conformations that are important for catalysis[36], and both of these are captured by the structures presented here (**Supplementary Fig. 1f–j**). Tet(50) monomer A, which has a closed substrate-loading channel, bound FAD in an IN conformation (**Fig. 2h**). In this conformation the reactive isoalloxazine moiety of the FAD is stretched away from the adenosine moiety and into the substrate-binding site. This allows a reaction with molecular oxygen to produce an FAD–hydroperoxide intermediate that is in close proximity to the tetracycline substrate (the C4a of FAD is ~5.9 Å away from the C11a substrate hydroxylation site in Tet(X)), allowing hydroxylation and subsequent spontaneous degradation of the tetracycline substrate[37]. After catalysis, FAD flips away from the substrate-binding site, adopting the OUT conformation. Tet(50) monomer B, which has an open substrate-loading channel, binds FAD in an OUT conformation in which the isoalloxazine moiety is bent toward the adenosine and away from the substrate-binding site (**Fig. 2i**). This conformational change allows for products to be released through the open channel and positions the oxidized FAD for reduction by NADPH in a distinct NADPH-binding site during cofactor regeneration (**Figs. 2j** and **3a**)[37]. After reduction, FAD is poised to flip back to the IN conformation for the next round of catalysis upon substrate binding. Our observation of FAD in both IN and OUT conformations implies that FAD exists in an equilibrium between the two states in the absence of substrate binding.

Substrate binding drives FAD and channel conversion

Since accessibility of the substrate-loading channel appeared to be dependent on the conformation of FAD in the Tet(50) crystal structures, we soaked Tet(50) with various tetracycline compounds. Surprisingly, chlortetracycline binds to Tet(50) in a ~180° rotated orientation in comparison to the orientation in which chlortetracycline and other tetracycline substrates (for example, iodtetracycline, minocycline or tigecycline) bind Tet(X)[27,38] (**Fig. 3a–d** and **Supplementary Fig. 2**). Tetracycline compounds have a four-ring system (labeled A–D; **Fig. 3a**,**c**), which has a distinctive three-dimensional architecture with a substantial bend between rings A and B, allowing for unambiguous modeling into the electron density. In the Tet(X)–chlortetracycline structure, the chlortetracycline D ring with the attached chlorine faces away from the substrate-binding site and toward bulk solvent (**Fig. 3c**,**d**). This places the C11a substrate hydroxylation site of ring C proximal to FAD. In the Tet(50)–chlortetracycline structure, the D-ring chlorine now faces FAD with the dimethylamine group of the A ring, making van

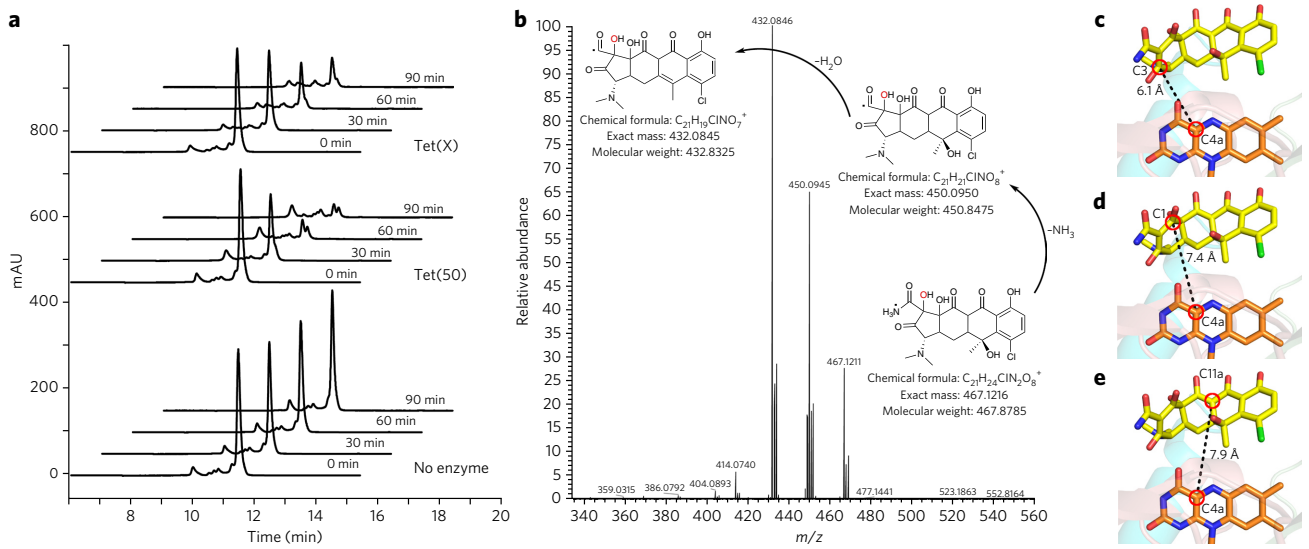

Figure 4 | Chlortetracycline is degraded by tetracycline destructases despite the unusual binding mode. (**a**) HPLC chromatograms show the time- and enzyme-dependent consumption of chlortetracycline. Reaction progress and enzyme indicated to the right of chromatograms. (**b**) High-resolution MS–MS analysis of the tetracycline-destructase reaction with chlortetracycline supports clean conversion to the *m/z* 467 oxidation product. MS–MS spectrum of the *m/z* 467 ion from the Tet(55) reaction with proposed fragmentation pathway. (**c**–**e**) The closest reactive carbons to C4a of the FAD cofactor are C3 (**c**) and C1 (**d**) of the chlortetracycline A ring, both of which are closer than C11a (**e**), the hydroxylation site observed in Tet(X)-mediated chlortetracycline degradation.

der Waals contacts with Phe95 from the flexible loop, with Val348 from the first C-terminal α-helix, and with Ile371 from the second C-terminal α-helix (**Fig. 3a**,**b**). Surprisingly, this new orientation positions C11a of chlortetracycline away from C4a of FAD.

We observed a second notable characteristic when comparing the structures of Tet(50) in the presence and absence of chlortetracycline. In the absence of chlortetracycline, Tet(50) monomer A had FAD in an IN conformation with a closed channel (**Fig. 2b**,**e**,**h**) and monomer B had FAD in an OUT conformation with an open channel (**Fig. 2c**,**f**,**i**). However, in the presence of chlortetracycline, we only detected bound chlortetracycline in monomer B, which now had FAD in an IN conformation and a closed channel (**Fig. 3e**–**h**). Thus, substrate binding to Tet(50) monomer B induced a conformational switch from FAD OUT to FAD IN, as well as loop closure (**Fig. 3h**,**i**).

Tetracycline destructases degrade chlortetracycline

Because of the unanticipated orientation of chlortetracycline binding, we examined whether the tetracycline destructases could degrade chlortetracycline. Enzymatic reactions were analyzed at several time points by reverse-phase HPLC. We observed the time- and enzyme-dependent degradation of chlortetracycline by Tet(50) and Tet(X) (**Fig. 4a**). Kinetic parameters of enzymatic inactivation were determined by monitoring *in vitro* reaction progress at an absorbance of 400 nm. The catalytic efficiency of Tet(50) was five times higher than that of Tet(X) (k_{cat}/K_m values of 0.55 and 0.11 μM/min, respectively) (**Supplementary Table 2**). This increased efficiency is primarily due to increased turnover, as the apparent K_m values are comparable between Tet(50) (6.3 ± 2.0 μM) and Tet(X) (7.9 ± 2.7 μM) despite their different substrate-binding orientations. Tet(55) and Tet(56) also degraded chlortetracycline *in vitro* with 4-fold and 15-fold greater efficiencies than Tet(X), respectively (**Supplementary Table 2**). Furthermore, *tet(50)*, *tet(51)*, *tet(55)*, *tet(56)*, and *tet(X)* each confer chlortetracycline resistance when expressed in *E. coli* at levels 16- to 32-fold greater than the vector-only control (**Supplementary Table 3**). As a result, despite employing a distinct mode of substrate binding, Tet(50), Tet(51), Tet(55), and Tet(56) are able to degrade chlortetracycline more efficiently than Tet(X).

Tetracycline inactivation by Tet(X) occurs via catalysis at C11a, resulting in a product that has a *m/z* of 461 (ref. 28). Because chlortetracycline binds Tet(50) in an alternative mode that positions C11a far away from the reactive flavin peroxide moiety, we sought to characterize the degradation product to establish substrate hydroxylation. Enzymatic reactions were analyzed by liquid chromatography–mass spectrometry (**Supplementary Fig. 3**) and were found to convert chlortetracycline (*m/z* 479) to an oxidation product with a *m/z* of 467. This result is in contrast to the *m/z* 461 monooxygenation product observed for tetracycline[28], and is consistent with an alternate binding mode for chlortetracycline. To further characterize this product, reactions were subjected to high-resolution MS (**Fig. 4b**). Reactions with each enzyme assayed (Tet(50), Tet(55), and Tet(56)) yielded a primary product with an exact *m/z* of 467.12 (**Supplementary Fig. 4a**–**d**).

In the alternative binding mode, the nonplanarity of the chlortetracycline substrate positions the reactive A-ring C3 in closest proximity to the flavin cofactor. Notably, the C3 is 6.1 Å (**Fig. 4c**) and the C1 carbonyl 7.4 Å (**Fig. 4d**) from the C4a of the flavin cofactor. These distances are similar to that between C11a of chlortetracycline and C4a of FAD in the Tet(X)–chlortetracycline structure[27] and are well within the C4a-reactive atom distances observed for flavin monooxygenases[39]. The C11a in the Tet(50)–chlortetracycline, on the other hand, is on the opposite side of the molecule, 7.9 Å away (**Fig. 4e**). Accordingly, we propose a mechanism in which the flavin peroxide attacks C3 of the chlortetracycline A ring, yielding intermediate **1** (**Supplementary Fig. 4e**). Spontaneous epoxide formation gives intermediates **2** and **3**, which then rearranges to a cycloheptanone intermediate **5** via Baeyer–Villiger ring expansion. Expulsion of carbon monoxide yields intermediate **6**, and ring contraction yields oxidation product **7**, which has a *m/z* of 467. Alternatively, intermediate **3** can be formed by flavin-peroxide attack of C1 of the chlortetracycline A ring, via intermediate **4**, and then similarly continue through products **5**–**7**. The final product **7** is consistent with the fragmentation pattern observed in tandem MS (**Fig. 4b**). Similar oxidative cascades proceeding through Baeyer–Villiger reactions have been observed in the biosynthesis of the cyclic type II polyketide mithramycin by the flavin monooxygenase MtmOIV[40]. The discovery of alternative substrate-binding modes and characterization of degradation products demonstrates the plasticity

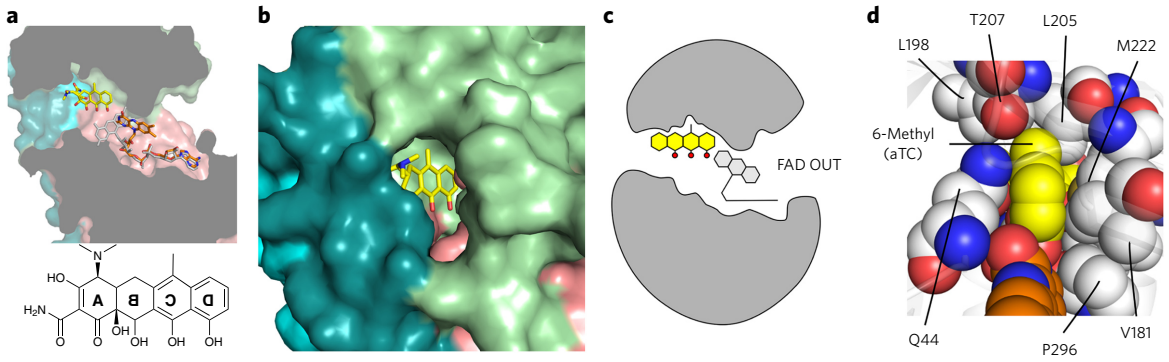

Figure 5 | Anhydrotetracycline binds to the active site of Tet(50), trapping FAD in the unproductive OUT conformation. (**a**) Anhydrotetracycline binds the active site of Tet(50) and traps the FAD cofactor in the unproductive OUT conformation (orange) in monomer B. The IN conformation of FAD from monomer A, superimposed in gray for comparison, sterically clashes with the D-ring hydroxyl of anhydrotetracycline. (**b**) Surface representation of Tet(50)–anhydrotetracycline reveals that the substrate-loading channel remains open, which corresponds to FAD locked in the OUT conformation. (**c**) In Tet(50)–anhydrotetracycline monomer B, FAD is OUT, the loop is open, and anhydrotetracycline is bound (not shown: in monomer A, FAD is IN, the loop is closed, and no anhydrotetracycline is bound). (**d**) Residue Thr207 in Tet(50) makes van der Waals interactions with the planar 6-methyl group of anhydrotetracycline (aTC) (yellow) in the bound orientation, but would sterically clash with the 6-methyl and 6-hydroxyl groups that branch from the C ring of tetracycline or chlortetracycline if bound in a flipped orientation.

of tetracycline destructases in adapting flavoenzyme-mediated degradation chemistries to achieve resistance in the presence of diverse tetracycline scaffolds.

Anhydrotetracycline locks the FAD in an OUT conformation

Because of the global dissemination of the β-lactamases, nearly all β-lactam antibiotics are co-developed with β-lactamase inhibitors[29], an approach that has successfully prolonged their clinical utility. We reasoned that a similar strategy might be useful to counteract tetracycline resistance by inactivation, and therefore sought to identify small-molecule inhibitors of these enzymes. Previously, we observed that anhydrotetracycline, a key biosynthetic precursor[41] and degradation product[42] of tetracycline that has poor antibiotic activity, was not degraded by Tet(47)–Tet(56)[28]. Nonetheless, it is known to be an effector of tetracycline producers and tetracycline-resistant bacteria by inducing expression of energetically expensive tetracycline efflux pumps, permitting tetracycline producers to survive, and selecting against tetracycline resistance[43]. On the basis of the structural similarity of anhydrotetracycline to tetracycline and intimate role that it plays in tetracycline biology, we hypothesized that anhydrotetracycline represents an evolutionarily privileged chemical lead for inhibitor design.

We obtained a co-crystal structure of Tet(50) that had anhydrotetracycline bound and observed two unique features compared to our Tet(50)–chlortetracycline and the earlier Tet(X)–chlortetracycline structures. First, anhydrotetracycline binds to Tet(50) in a flipped orientation and in a position distinct from where chlortetracycline binds (**Fig. 5a–c** and **Supplementary Figs. 5** and **6**). This unique binding mode is enabled by anhydrotetracycline's lack of a 6-hydroxyl group of ring C, which is present in tetracycline and chlortetracycline (**Fig. 5a**). Without this substitution at the 6 position, the tetracycline gains additional aromatic stabilization. The resultant planar structure allows the 6-methyl group to make van der Waals interactions with a conserved threonine or serine at residue position 207 in Tet(47)–Tet(56) (**Fig. 5d** and **Supplementary Figs. 6** and **7**). Thr207 would cause a steric clash with the 6-methyl and 6-hydroxyl groups of ring C in tetracycline or chlortetracycline, explaining their distinct binding modes.

The second interesting feature is that when anhydrotetracycline was bound, FAD was in the OUT conformation and the substrate-loading channel was open (**Fig. 5b**,**c**). The unique binding location of anhydrotetracycline locks the isoalloxazine moiety of FAD away from the substrate-binding site and sterically blocks the transition to the FAD IN conformation observed in the Tet(50)–chlortetracycline monomer B. This unexpected binding mode establishes a novel mechanism for inhibitors that stabilize the inactive OUT conformation of the FAD cofactor in flavoenzymes and prevents transition to the necessary FAD IN conformation for catalysis. Therefore, anhydrotetracycline is a mechanistic inhibitor of the tetracycline destructases that also competitively blocks substrate binding.

Anhydrotetracycline inhibits tetracycline destructases

We examined the effect of anhydrotetracycline on tetracycline destructase activity *in vitro*. We performed *in vitro* enzymatic reactions in the presence and absence of anhydrotetracycline followed by HPLC. For clinical relevance, we first focused on Tet(56), the tetracycline destructase from pathogenic *L. longbeachae*. We observed the Tet(56)-dependent degradation of 0.1 mM tetracycline over time, as demonstrated by the decrease in the tetracycline peak (**Fig. 6a**). However, in the presence of 1 mM anhydrotetracycline, the tetracycline peak does not change, indicating that tetracycline is not degraded (**Fig. 6b**). Similar results were observed for Tet(50), Tet(51), Tet(55) and Tet(X) (**Supplementary Fig. 8**; **Supplementary Table 4**). We also monitored enzymatic inactivation of tetracycline at an absorbance of 400 nm in the presence of a range of anhydrotetracycline concentrations. Anhydrotetracycline inhibited Tet(50), Tet(55), and Tet(56) with half-maximal inhibitory concentrations (IC_{50}s) of 83.2 ± 1.2 μM, 25.6 ± 1.2 μM, and 37.1 ± 1.1 μM, respectively (**Fig. 6c**). Thus, anhydrotetracycline prevents the enzyme-dependent degradation of tetracycline. Together with our structural data, this indicates a common mechanism of inhibition for tetracycline-inactivating enzymes and establishes anhydrotetracycline as a lead compound that presents a flexible starting point for generating tetracycline destructase inhibitors with improved activity[44]. This inhibition strategy, which stabilizes inactive cofactor states, is widely applicable to the larger superfamily of flavoenzymes and offers new avenues for inhibiting any member of this superfamily, many of which have been implicated in human disease and represent promising targets for hypercholesterolemia and antifungal drugs[45].

Novel inhibition mechanism restores tetracycline activity

Our data suggest that a combination therapy strategy using a tetracycline and a tetracycline destructase inhibitor (for example, anhydrotetracycline) could potentially be employed to rescue antibiotic activity of tetracyclines against bacteria that possess tetracycline-inactivating enzymes. Tet(X) and Tet(56) are of particular interest

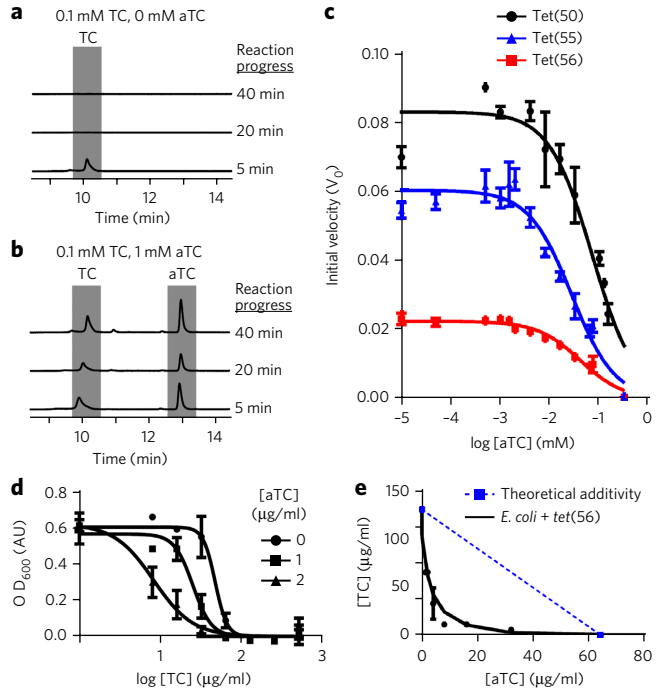

Figure 6 | Anhydrotetracycline prevents enzymatic tetracycline degradation, functionally rescuing tetracycline antibiotic activity. (**a**) TC is degraded by Tet(56) *in vitro*. HPLC chromatograms show *in vitro* reactions with UV detection at 363 nm and separation on a C18 column. (**b**) TC degradation is attenuated by the addition of an excess of aTC. (**c**) Dose-dependent inhibition of Tet(50), Tet(55), and Tet(56) activity by anhydrotetracycline. Velocity is determined by measuring tetracycline consumption via change in absorbance at 400 nm. Data are represented as mean ± s.d. of three technical replicates. (**d**) Dose–response curve showing the effect of aTC on sensitivity of Tet(56)-expressing *E. coli* to TC in liquid culture. Data are represented as mean ± s.e.m. of three technical replicates. (**e**) TC and aTC synergistically inhibit growth of *E. coli* expressing Tet(56); FICI = 0.1875. Points show minimum inhibitory concentrations of two drugs in combination. Dashed line indicates the theoretical concentration of additive drug interaction. Data represented as mean ± s.e.m. of three technical replicates.

because of their clinical importance. *tet*(X) has been recently identified in a number of human pathogens, including 11 nosocomial uropathogens from Sierra Leone[46] and 12 *Acinetobacter baumannii* isolates from a hospital in China[47]. We also showed that *tet*(56) is present and functional in *L. longbeachae*[28]—a pathogen responsible for causing Pontiac fever and Legionnaires' disease[32,33]. Accordingly, we tested whether anhydrotetracycline rescues tetracycline efficacy against *E. coli* expressing *tet*(56). Two micrograms per milliliter of anhydrotetracycline caused a greater than five-fold change in sensitivity of *E. coli* expressing *tet*(56) to tetracycline in liquid culture, as indicated by a change in IC_{50} from 47.4 to 8.27 μg/ml (**Fig. 6d**). Furthermore, anhydrotetracycline and tetracycline acted synergistically to inhibit growth of *E. coli* expressing Tet(50), Tet(51), Tet(55), and Tet(56), with fractional inhibitory concentration indices (FICI) of 0.625, 0.5, 0.375 and 0.1875, respectively (**Fig. 6e** and **Supplementary Fig. 9**). Although anhydrotetracycline is not degraded by Tet(47)–Tet(56), it is slowly degraded by Tet(X)[28]. However, anhydrotetracycline still was able to prevent tetracycline degradation by Tet(X) *in vitro* (**Supplementary Fig. 8**). Our proof-of-concept experiment, taken together with our structural and *in vitro* data, reveals that a co-administration strategy based on inhibition of tetracycline-inactivating enzymes could be effective for the treatment of tetracycline-resistant bacterial infections.

DISCUSSION

The widespread anthropogenic use of tetracycline antibiotics motivates the immediate study of emerging mechanisms of tetracycline resistance, such as enzymatic inactivation. Our data provide unprecedented insight into the dynamics of tetracycline-inactivating enzymes and reveal a novel mode of inhibition. Substrates like chlortetracycline are loaded into enzymes in the FAD OUT conformation through the substrate-loading channel (**Supplementary Fig. 10a**), which is opened as a flexible loop is pulled away from the channel. Upon substrate binding the enzyme converts to FAD IN, the channel closes, and catalysis can occur because of the proximity of FAD to the substrate. Mechanistic inhibitors like anhydrotetracycline also enter the enzyme through the same channel, but they bind at a distinct site (**Supplementary Fig. 10b**). Binding of inhibitor in this location sterically blocks FAD conversion to the IN conformation and prevents subsequent substrate binding and catalysis. Our model predicts that compounds that either bind with higher affinity to the inhibitor-binding pocket or concomitantly bind to the inhibitor and substrate-binding sites will provide enhanced inhibition for the control of tetracycline resistance. This novel mechanism of inhibition is not only applicable to the prevention of antibiotic resistance, but is highly relevant to the study of additional FAD-dependent enzymes that comprise the flavoenzyme superfamily and are of clinical interest[45].

The rise in resistance to early-generation tetracyclines has spurred the development of next-generation derivatives, including tigecycline (approved for human use in 2005)[15] and eravacycline and omadacycline (currently in late-stage clinical trials)[16,17]. These newer drugs are designed to evade resistance by efflux or ribosomal protection, but they are largely untested against tetracycline-inactivating enzymes. Alarmingly, tigecycline was found to be vulnerable to oxidative inactivation by Tet(X)[27], which was recently identified for the first time in numerous pathogens of high clinical concern[46,47]. These challenges highlight the immediate importance of studying mechanisms of emerging tetracycline resistance, such as those described here, that expand substrate scope.

Tetracycline resistance by enzymatic inactivation has thus far been rarely documented compared to resistance by efflux or ribosomal protection. Growing evidence, however, indicates that enzymatic tetracycline inactivation is a widespread feature in soil microbial communities[28] and is a recently observed emerging threat in human pathogens[46–48]. Flavoenzymes display a proclivity for horizontal gene transfer and gene duplication, bestowing the potential to spread between bacteria and acquire new functions[49]. Interestingly, the contigs on which *tet*(47)–*tet*(55) were discovered also contained mobility elements and other resistance genes[9,28], suggesting that their original genomic context may be as part of a multidrug resistance cassette or mobile genetic element. This indicates that tetracycline-inactivating enzymes pose a threat for facile acquisition by additional human pathogens. Indeed, we show that *tet*(56) is present and functional in the human pathogen *L. longbeachae*, and *tet*(X) has now been reported in four out of six ESKAPE pathogens[46–48], demonstrating the urgency of this threat. Our results reveal the structural basis for plasticity and dynamics in substrate binding in these enzymes. We propose a new combination-therapy strategy to retain tetracycline efficacy against bacteria that harbor tetracycline-inactivating resistance genes. Our results provide the structural and biochemical foundation to counter the alarming emergence of tetracycline resistance via enzymatic inactivation.

Received 1 September 2016; accepted 8 February 2017; published online 8 May 2017

METHODS

Methods, including statements of data availability and any associated accession codes and references, are available in the online version of the paper.

References

1. Knapp, C.W., Dolfing, J., Ehlert, P.A. & Graham, D.W. Evidence of increasing antibiotic resistance gene abundances in archived soils since 1940. *Environ. Sci. Technol.* **44**, 580–587 (2010).
2. Kinch, M.S., Patridge, E., Plummer, M. & Hoyer, D. An analysis of FDA-approved drugs for infectious disease: antibacterial agents. *Drug Discov. Today* **19**, 1283–1287 (2014).
3. Davies, J. Inactivation of antibiotics and the dissemination of resistance genes. *Science* **264**, 375–382 (1994).
4. Allen, H.K. *et al.* Call of the wild: antibiotic resistance genes in natural environments. *Nat. Rev. Microbiol.* **8**, 251–259 (2010).
5. Berendonk, T.U. *et al.* Tackling antibiotic resistance: the environmental framework. *Nat. Rev. Microbiol.* **13**, 310–317 (2015).
6. Benveniste, R. & Davies, J. Aminoglycoside antibiotic-inactivating enzymes in actinomycetes similar to those present in clinical isolates of antibiotic-resistant bacteria. *Proc. Natl. Acad. Sci. USA* **70**, 2276–2280 (1973).
7. D'Costa, V.M. *et al.* Antibiotic resistance is ancient. *Nature* **477**, 457–461 (2011).
8. Forsberg, K.J. *et al.* The shared antibiotic resistome of soil bacteria and human pathogens. *Science* **337**, 1107–1111 (2012).
9. Forsberg, K.J. *et al.* Bacterial phylogeny structures soil resistomes across habitats. *Nature* **509**, 612–616 (2014).
10. Yong, D. *et al.* Characterization of a new metallo-β-lactamase gene, bla(NDM-1), and a novel erythromycin esterase gene carried on a unique genetic structure in *Klebsiella pneumoniae* sequence type 14 from India. *Antimicrob. Agents Chemother.* **53**, 5046–5054 (2009).
11. Liu, Y.Y. *et al.* Emergence of plasmid-mediated colistin resistance mechanism MCR-1 in animals and human beings in China: a microbiological and molecular biological study. *Lancet Infect. Dis.* **16**, 161–168 (2016).
12. Poirel, L., Rodriguez-Martinez, J.M., Mammeri, H., Liard, A. & Nordmann, P. Origin of plasmid-mediated quinolone resistance determinant QnrA. *Antimicrob. Agents Chemother.* **49**, 3523–3525 (2005).
13. Thaker, M., Spanogiannopoulos, P. & Wright, G.D. The tetracycline resistome. *Cell. Mol. Life Sci.* **67**, 419–431 (2010).
14. State of the World's Antibiotics. 2015. (Center for Disease Dynamics, Economics & Policy, Washington, DC, USA, 2015).
15. Kasbekar, N. Tigecycline: a new glycylcycline antimicrobial agent. *Am. J. Health Syst. Pharm.* **63**, 1235–1243 (2006).
16. Sutcliffe, J.A., O'Brien, W., Fyfe, C. & Grossman, T.H. Antibacterial activity of eravacycline (TP-434), a novel fluorocycline, against hospital and community pathogens. *Antimicrob. Agents Chemother.* **57**, 5548–5558 (2013).
17. Macone, A.B. *et al. In vitro* and *in vivo* antibacterial activities of omadacycline, a novel aminomethylcycline. *Antimicrob. Agents Chemother.* **58**, 1127–1135 (2014).
18. Chopra, I. & Roberts, M. Tetracycline antibiotics: mode of action, applications, molecular biology, and epidemiology of bacterial resistance. *Microbiol. Mol. Biol. Rev.* **65**, 232–260 (2001).
19. Park, B.H. & Levy, S.B. The cryptic tetracycline resistance determinant on Tn4400 mediates tetracycline degradation as well as tetracycline efflux. *Antimicrob. Agents Chemother.* **32**, 1797–1800 (1988).
20. Speer, B.S. & Salyers, A.A. Characterization of a novel tetracycline resistance that functions only in aerobically grown *Escherichia coli*. *J. Bacteriol.* **170**, 1423–1429 (1988).
21. Whittle, G., Hund, B.D., Shoemaker, N.B. & Salyers, A.A. Characterization of the 13-kilobase ermF region of the Bacteroides conjugative transposon CTnDOT. *Appl. Environ. Microbiol.* **67**, 3488–3495 (2001).
22. Nonaka, L. & Suzuki, S. New Mg^{2+}-dependent oxytetracycline resistance determinant tet 34 in Vibrio isolates from marine fish intestinal contents. *Antimicrob. Agents Chemother.* **46**, 1550–1552 (2002).
23. Diaz-Torres, M.L. *et al.* Novel tetracycline resistance determinant from the oral metagenome. *Antimicrob. Agents Chemother.* **47**, 1430–1432 (2003).
24. Ghosh, S., Sadowsky, M.J., Roberts, M.C., Gralnick, J.A. & LaPara, T.M. Sphingobacterium sp. strain PM2-P1-29 harbours a functional tet(X) gene encoding for the degradation of tetracycline. *J. Appl. Microbiol.* **106**, 1336–1342 (2009).
25. Yang, W. *et al.* TetX is a flavin-dependent monooxygenase conferring resistance to tetracycline antibiotics. *J. Biol. Chem.* **279**, 52346–52352 (2004).
26. Moore, I.F., Hughes, D.W. & Wright, G.D. Tigecycline is modified by the flavin-dependent monooxygenase TetX. *Biochemistry* **44**, 11829–11835 (2005).
27. Volkers, G., Palm, G.J., Weiss, M.S., Wright, G.D. & Hinrichs, W. Structural basis for a new tetracycline resistance mechanism relying on the TetX monooxygenase. *FEBS Lett.* **585**, 1061–1066 (2011).
28. Forsberg, K.J., Patel, S., Wencewicz, T.A. & Dantas, G. The tetracycline destructases: a novel family of tetracycline-inactivating enzymes. *Chem. Biol.* **22**, 888–897 (2015).
29. Drawz, S.M., Papp-Wallace, K.M. & Bonomo, R.A. New β-lactamase inhibitors: a therapeutic renaissance in an MDR world. *Antimicrob. Agents Chemother.* **58**, 1835–1846 (2014).
30. Hornak, V., Okur, A., Rizzo, R.C. & Simmerling, C. HIV-1 protease flaps spontaneously close to the correct structure in simulations following manual placement of an inhibitor into the open state. *J. Am. Chem. Soc.* **128**, 2812–2813 (2006).
31. Pesnot, T., Jørgensen, R., Palcic, M.M. & Wagner, G.K. Structural and mechanistic basis for a new mode of glycosyltransferase inhibition. *Nat. Chem. Biol.* **6**, 321–323 (2010).
32. Cazalet, C. *et al.* Analysis of the *Legionella longbeachae* genome and transcriptome uncovers unique strategies to cause Legionnaires' disease. *PLoS Genet.* **6**, e1000851 (2010).
33. Whiley, H. & Bentham, R. *Legionella longbeachae* and legionellosis. *Emerg. Infect. Dis.* **17**, 579–583 (2011).
34. Ballou, D.P., Entsch, B. & Cole, L.J. Dynamics involved in catalysis by single-component and two-component flavin-dependent aromatic hydroxylases. *Biochem. Biophys. Res. Commun.* **338**, 590–598 (2005).
35. van Berkel, W.J., Kamerbeek, N.M. & Fraaije, M.W. Flavoprotein monooxygenases, a diverse class of oxidative biocatalysts. *J. Biotechnol.* **124**, 670–689 (2006).
36. Gatti, D.L. *et al.* The mobile flavin of 4-OH benzoate hydroxylase. *Science* **266**, 110–114 (1994).
37. Massey, V. Activation of molecular oxygen by flavins and flavoproteins. *J. Biol. Chem.* **269**, 22459–22462 (1994).
38. Volkers, G. *et al.* Putative dioxygen-binding sites and recognition of tigecycline and minocycline in the tetracycline-degrading monooxygenase TetX. *Acta Crystallogr. D Biol. Crystallogr.* **69**, 1758–1767 (2013).
39. Liu, L.K. *et al.* The structure of the antibiotic deactivating, N-hydroxylating rifampicin monooxygenase. *J. Biol. Chem.* **291**, 21553–21562 (2016).
40. Gibson, M., Nur-e-alam, M., Lipata, F., Oliveira, M.A. & Rohr, J. Characterization of kinetics and products of the Baeyer–Villiger oxygenase MtmOIV, the key enzyme of the biosynthetic pathway toward the natural product anticancer drug mithramycin from Streptomyces argillaceus. *J. Am. Chem. Soc.* **127**, 17594–17595 (2005).
41. Wang, P., Bashiri, G., Gao, X., Sawaya, M.R. & Tang, Y. Uncovering the enzymes that catalyze the final steps in oxytetracycline biosynthesis. *J. Am. Chem. Soc.* **135**, 7138–7141 (2013).
42. Yuen, P.H. & Sokoloski, T.D. Kinetics of concomitant degradation of tetracycline to epitetracycline, anhydrotetracycline, and epianhydrotetracycline in acid phosphate solution. *J. Pharm. Sci.* **66**, 1648–1650 (1977).
43. Palmer, A.C., Angelino, E. & Kishony, R. Chemical decay of an antibiotic inverts selection for resistance. *Nat. Chem. Biol.* **6**, 105–107 (2010).
44. Liu, F. & Myers, A.G. Development of a platform for the discovery and practical synthesis of new tetracycline antibiotics. *Curr. Opin. Chem. Biol.* **32**, 48–57 (2016).
45. Lienhart, W.D., Gudipati, V. & Macheroux, P. The human flavoproteome. *Arch. Biochem. Biophys.* **535**, 150–162 (2013).
46. Leski, T.A. *et al.* Multidrug-resistant tet(X)-containing hospital isolates in Sierra Leone. *Int. J. Antimicrob. Agents* **42**, 83–86 (2013).
47. Deng, M. *et al.* Molecular epidemiology and mechanisms of tigecycline resistance in clinical isolates of *Acinetobacter baumannii* from a Chinese university hospital. *Antimicrob. Agents Chemother.* **58**, 297–303 (2014).
48. Boucher, H.W. *et al.* Bad bugs, no drugs: no ESKAPE! An update from the Infectious Diseases Society of America. *Clin. Infect. Dis.* **48**, 1–12 (2009).
49. Walsh, C.T. & Wencewicz, T.A. Flavoenzymes: versatile catalysts in biosynthetic pathways. *Nat. Prod. Rep.* **30**, 175–200 (2013).

Acknowledgments

We thank J. Nix and ALS beamline 4.2.2 (contract DE-AC02-05CH11231) for assistance with X-ray data collection and A. Durairaj of the Proteomics & Mass Spectrometry Facility at the Danforth Plant Science Center for assistance with HR–MS/MS experiments. This work was supported by an award to N.H.T., G.D., and T.A.W. from the National Institute of Allergy and Infectious Diseases of the National Institutes of Health (R01 AI123394). A.J.G. is supported by the National Institute of General Medical Sciences Cell and Molecular Biology Training Grant (T32 GM007067). The content is solely the responsibility of the authors and does not necessarily represent the official views of the funding agencies.

Author contributions

J.P. designed and performed crystallographic experiments and X-ray structure determination, analyzed data, and wrote the paper; A.J.G. designed and performed *in vitro* and microbiological experiments, analyzed data, and wrote the paper; M.R.R. and C.T.S. performed *in vitro* experiments; J.L.E. performed crystallographic experiments; J.P.V. performed *Legionella* experiments; T.A.W., G.D., and N.H.T. designed experiments, analyzed data, and wrote the manuscript.

Competing financial interests

The authors declare no competing financial interests.

Additional information

Any supplementary information, chemical compound information and source data are available in the online version of the paper. Reprints and permissions information is available online at http://www.nature.com/reprints/index.html. Publisher's note: Springer Nature remains neutral with regard to jurisdictional claims in published maps and institutional affiliations. Correspondence and requests for materials should be addressed to N.H.T., G.D. or T.A.W.

ONLINE METHODS

***Legionella* plasmid construction.** The Tet(56) deletion plasmid pJB7204 was constructed by amplifying 2 kb of DNA upstream and downstream of the Tet(56) open reading frame (ORF) using primers JVP2913/JVP2910 and JVP2911/JVP2912 and *Legionella longbeachae* chromosomal DNA. The PCR products were digested with SalI/NotI and NotI/SacI, respectively, and ligated into SalI/SacI-digested suicide vector pSR47S[50]. The ligated product was transformed into EC100D::Δpir and selected on LB medium plates containing 20 μg/ml kanamycin. The Tet(56) complementing clone pJB7207 was constructed by amplifying the Tet(56) ORF using primers JVP2921/JVP2922 and *Legionella longbeachae* chromosomal DNA. The PCR product was digested with BamHI/SalI and cloned into BamHI/SalI-digested expression vector pJB1625 (**Supplementary Table 5**).

***Legionella* strain construction.** The Tet(56) deletion strain JV8858 was constructed by a traditional loop-in/loop-out strategy. Briefly, the wild-type *Legionella longbeachae* strain JV595 was transformed by electroporation with the ΔTet(56) suicide plasmid pJB7204, and integrants were selected on charcoal yeast extract (CYE) plates[51] containing 30 μg/ml kanamycin. Resolution of the merodiploid was obtained on CYE plates containing sucrose. Strains were then electroporated with the vector pJB1625 or the Tet(56) complementing clone pJB7207, and transformants were selected on CYE plates containing 5 μg/ml chloramphenicol.

Tetracycline inactivation in *Legionella*. Antibiotic susceptibility testing was performed using *L. longbeachae* wild-type and deletion strains and *L. pneumophila*[52], bearing either the vector pJB1625 (ref. 53) or the Tet(56) complementing clone pJB7207. Minimum inhibitory concentrations were determined according to Clinical and Laboratory Standards Institute (CLSI) procedures with the following modifications. Results are representative of three independent experiments. The strains were initially grown as a patch on CYE plates containing chloramphenicol for 2 d at 37 °C. The bacteria were swabbed into distilled water, washed one time, and resuspended at a 600 nm absorbance (OD_{600}) of 1 (~1E9 CFU/ml). The culture was diluted 200-fold into 10 ml of buffered AYE media containing 2 μg/ml chloramphenicol and a range of tetracycline, but without supplemental iron, as iron can interfere with tetracycline activity. The cultures were grown for 48 h at 37 °C on a roller drum, and the absorbances (OD_{600}) were periodically measured using a Genesys 20 Spectrophotometer.

Cloning, expression and purification of tetracycline-inactivating enzymes. All genes encoding tetracycline-inactivating enzymes were cloned into the pET28b(+) vector (Novagen) at BamHI and NdeI restriction sites. Constructs were transformed into BL21-Star (DE3) competent cells (Life Technologies). Cells harboring the plasmid were grown at 37 °C in LB medium containing a final concentration of 0.03 mg/ml kanamycin. Once cells reached an OD_{600} of 0.6, cells were cooled to 15 °C and induced with 1 mM IPTG overnight. After this period, cells were harvested by centrifugation at 4,000 r.p.m. for 10 min at 4 °C. Cell pellets were resuspended in 10 ml of 50 mM Tris (pH 8.0), 100 mM NaCl, 10 mM imidazole (pH 8.0), 1 mM PMSF, and 5 mM BME per 1 L of LB medium and stored at −80 °C.

Cells were thawed in the presence of 0.25 mg/ml lysozyme and disrupted using sonication on ice for 60 s. The cell extract was obtained by centrifugation at 13,000 r.p.m. for 30 min at 4 °C and was applied onto nickel rapid run agarose beads (Goldbio) equilibrated with wash buffer (50 mM Tris (pH 8.0), 150 mM NaCl, 20 mM imidazole (pH 8.0), and 5 mM BME). The wash buffer was used to wash the nickel column three times with five column volumes. After washing, protein was eluted with five column volumes of elution buffer (wash buffer with 300 mM imidazole). The protein sample was further purified by gel chromatography using a HiLoad 16/600 Superdex 200 pg column (GE Healthcare) equilibrated with 10 mM Tris (pH 8.0), 150 mM NaCl, 5 mM DTT. The fractions containing the protein of interest were pooled and concentrated using a 30 K MWCO Amicon centrifugal filter (Millipore).

Tet(55) selenomethionine labeling. For selenomethionine-labeled Tet(55) (Se-Met Tet(55)), cells were grown in 1 L of SelenoMet Medium supplemented with SelenoMet Nutrient Mix (Molecular Dimensions Limited). Once cells reached an OD_{600} of 0.6, feedback inhibition amino acid mix (0.1 g of lysine, threonine, phenylalanine; 0.05 g of leucine, isoleucine, valine; 0.05 g of L-(+)-selenomethionine (ACROS Organics 259960025)) was added, and the cells were shaken for 15 min at 15 °C. After 15 min, cells were induced at 15 °C with 1 mM IPTG overnight. All other purification conditions were the same as for the native tetracycline-inactivating enzymes.

Crystallization, data collection, and structure determination. For crystallization, Se-Met Tet(55) was concentrated to 25 mg/ml. Crystals were obtained by vapor diffusion using hanging drops equilibrated at 18 °C. Se-Met Tet(55) was crystallized in 0.1 M Tris–HCl (8.5) and 20–25% PEG 3000. Se-Met Tet(55) crystals were harvested directly from the growth condition and flash frozen under liquid nitrogen.

Native Tet(55) was concentrated to 50 mg/ml and crystallized in 0.1 M Tris–HCl (8.5) and 25–27% PEG 4000. Native Tet(55) crystals were harvested directly from the growth condition and flash frozen. Tet(50) was concentrated to 35 mg/ml and crystallized in 0.1 M MES (pH 6.0–6.5), 1.6–2.0 M ammonium sulfate, 2–10% 1,4-dioxane. Crystals were harvested directly from the growth condition and flash frozen. For co-crystal structures, Tet(50) was concentrated to 17 mg/ml, and Tet(50) crystals were soaked with mother liquor plus 5 mM chlortetracycline or 4 mM anhydrotetracycline for 30 min before flash freezing. Tet(51) was concentrated to 13 mg/ml and crystallized in 0.1 M MES (pH 6.0) and 10% PEG 6000. Crystals were cryo-protected with 0.1 M MES (pH 6.0), 10% PEG 6000, and 30% glycerol before flash freezing. Tet(56) was concentrated to 38 mg/ml and crystallized in 0.1 M trisodium citrate (pH 5.6), 10% PEG 4000, and 10% isopropanol. Tet(56) crystals were cryo-protected in 0.1 M trisodium citrate (pH 5.6), 10% PEG 4000, 10% isopropanol, and 20% glycerol before flash freezing.

The crystal structure of Tet(55) was solved by Se-Met labeling and single-wavelength anomalous dispersion (SAD) (**Supplementary Table 1**), as molecular replacement using the previously published Tet(X) structures was unsuccessful. The inability to solve the structure by molecular replacement demonstrates that tetracycline-inactivating enzymes are structurally diverse, and multiple structures are required to capture the diversity within the family. X-ray data for selenomethionine-labeled Tet(55) were collected from a single crystal using a wavelength of 0.976289 Å at synchrotron beamline 4.2.2 of the Advanced Light Source in Berkeley, CA. All other native data sets were collected at a wavelength of 1 Å. Data were collected on the CMOS detector and were processed with XDS[54]. Structure solution for Se-Met Tet(55) was performed using PHENIX AutoSol. Thirteen selenium sites were found, which gave a figure of merit of 0.370. The resulting Tet(55) model was refined against the native Tet(55) data set. R and R_{free} flags were imported from the Se-Met Tet(55) MTZ file using UNIQUEIFY within the CCP4 package[55]. Tet(50,51,56) structures were solved by PHENIX AutoMR using an ensemble of three domains of Tet(55) (domain 1 = aa 1–70, aa100–172, aa 276–319; domain 2 = aa 71–99, 173–275; domain 3 = aa 320–387). Structure solution for the Tet(50) chlortetracycline and anhydrotetracycline structures were performed by refinement with the apo-Tet(50) structure, from which the R and R_{free} flags were imported using UNIQUEIFY.

Subsequent iterated manual building/rebuilding and refinement of models were performed using Coot[56] and PHENIX[57], respectively. The structure validation server MolProbity[58] was used to monitor refinement of the models. All final refined models have favorable crystallographic refinement statistics, as provided in **Supplementary Table 1**. Figures were generated and rendered in the PyMOL Molecular Graphics System (Version 0.99rc6, Schrödinger, LLC).

***In vitro* tetracycline and chlortetracycline inactivation assays.** Reactions were prepared in 100 mM TAPS buffer with 100 μM substrate, 14.4 μM enzyme, and an NADPH regenerating system consisting of the following components (final concentrations): glucose-6-phosphate (40 mM), $NADP^+$ (4 mM), $MgCl_2$ (1 mM), and glucose-6-phosphate dehydrogenase (4 U/ml). The regeneration system was incubated at 37 °C for 30 min to generate NADPH before use in reactions. Reactions were sampled at various time points and quenched in four volumes of an acidic quencher consisting of equal parts acetonitrile and 0.25 M HCl.

doi:10.1038/nchembio.2376

Products generated from enzymatic inactivation of both tetracycline and chlortetracycline were separated by reverse-phase HPLC using a Phenomenex Luna C18 column (5 µm, 110 Å, 2 × 50 mm) and 0.1% trifluoroacetic acid in water (A) and acetonitrile (B) as mobile phase. Injections of 25 µl sample volume were eluted using a linear gradient from 25% B to 75% B over 14 min at a flow rate of 1 ml/min.

Chlortetracycline reactions analyzed by high-resolution tandem MS were sampled at 75 min. The quenched samples were diluted 6× with 50% methanol in 0.1% formic acid and run on the Q Exactive Orbitrap by direct infusion using the Advion TriVersa NanoMate. The data were acquired with resolution of 140,000. The MS scan was acquired from *m/z* 300–550. MS/MS spectra were acquired on the *m/z* 467.12 compounds.

Tetracycline inactivation in *E. coli*. Antibiotic susceptibility testing was performed in *E. coli* MegaX cells (Invitrogen) bearing the pZE21 expression vector with the tetracycline inactivating gene of interest. Minimum inhibitory concentrations were determined according to Clinical and Laboratory Standards Institute (CLSI) procedures[59] using Mueller–Hinton broth with 50 µg/ml kanamycin and a range of chlortetracycline concentrations profiled via absorbance measurements at 600 nm (OD_{600}) at 45 min intervals using the Synergy H1 microplate reader (Biotek Instruments, Inc) for 48 h at 37 °C.

Kinetic characterization of tetracycline and chlortetracycline inactivation. The optimal enzyme concentration for steady state kinetics assays was determined by varying the concentration of enzyme while keeping chlortetracycline and NADPH concentration constant. 0.4 µM enzyme was found to give linear slopes for all concentrations of substrate tested, and this was used as the enzyme concentration for all kinetics experiments.

Reactions were prepared in 100 mM TAPS buffer at pH 8.5 with 0–160 µM substrate, 1.6 mM NADPH, and 0.4 µM enzyme. UV-visible spectroscopy measurements were taken in triplicate at 400 nm wavelength light with a Cary 60 UV-Vis system (Agilent) for 10 min at room temperature. Initial reaction velocities were determined by linear regression using the Agilent Cary WinUV Software and fitted to the Michaelis–Menten equation:

$$v_0 = \frac{V_{max}[S]}{K_m + [S]}$$

using GraphPad Prism 6.

LC–MS characterization of chlortetracycline degradation products. Reactions were prepared in 100 mM phosphates buffer at pH 8.5 with 1 mM CTC, 0.5 mM NADPH, 5 mM MgCl2, and 0.4 µM Tet(55). After 10 min, the reaction was centrifuge filtered for 10 min using a Millipore Amicon Ultracel (3 kDa MW cutoff) to remove enzyme. Prior to centrifugation, filters were triply rinsed with phosphate buffer to remove excess glycerol. The filtrate was collected and analyzed by LC–MS using an Agilent 6130 single quadrupole instrument with G1313 autosampler, G1315 diode array detector, and 1200 series solvent module. Reaction products were separated using a Phenomenex Gemini C18 column, 50 × 2 mm (5 µm) with guard column cassette was used with a linear gradient of 0% acetonitrile + 0.1% formic acid to 95% acetonitrile + 0.1% formic acid over 14 min at a flow rate of 0.5 ml/min before analysis by electrospray ionization.

***In vitro* characterization of anhydrotetracycline inhibition.** IC_{50} values were determined for Tet(50), Tet(55), and Tet(56) by measuring the initial velocity of tetracycline degradation in the presence of varying concentrations of anhydrotetracycline. The concentrations of tetracycline and NADPH were kept constant at 25 µM and 500 µM, respectively. Assays were prepared by combining all components except for enzyme and equilibrating to 25 °C for 5 min. After the addition of enzyme, absorbance at 400 nm was measured for 5 min. All measurements were taken in triplicate. The final concentrations for assay components were 100 mM TAPS buffer (pH 8.5), 25 µM tetracycline, 500 µM NADPH, 16 mM $MgCl_2$, 0.4 µM enzyme, and 0.05–150 µM anhydrotetracycline. A control assay using no anhydrotetracycline was assigned a concentration of 1.0×10^{-15} µM for analysis. A second control using no enzyme and 100 µM anhydrotetracycline was assigned a concentration of 1.0×10^{15} µM to simulate full inhibition of enzyme. IC_{50} values were determined by plotting the log of anhydrotetracycline concentration against v_0 in GraphPad Prism 6. Functional Tet(51) expressed poorly, so Tet(51) was omitted from these and other *in vitro* experiments.

Checkerboard synergy assay. Tetracycline (1,024 µg/ml) and anhydrotetracycline (256 µg/ml) were dissolved in cation-adjusted Mueller–Hinton broth supplemented with 50 µg/ml kanamycin. A two-fold dilution series of each drug was made independently across 8 rows of a 96-well master plate before 100 µl of each drug dilution series were combined into a 96-well culture plate (Costar), with rows included for no-drug and no-inocula controls. A sterile 96-pin replicator (Scinomix) was used to inoculate plates with ~1 µl of *E. coli* MegaX (Invitrogen) expressing a tetracycline inactivating enzyme, diluted to OD_{600} 0.1 using. Plates were sealed with Breathe-Easy membranes (Sigma-Aldrich) and incubated at 37 °C with shaking at 220 r.p.m. Endpoint growth was determined by OD_{600} at 20 and 36 h of growth using a Synergy H1 plate reader (BioTek, Inc.). Three independent replicates were performed for each strain on separate days. Synergy of anhydrotetracycline and tetracycline combinations was determined using the fractional inhibitory concentration index (FICI) method[60],

$$FICI = \frac{MIC\,A_{combo}}{MIC\,A_{alone}} + \frac{MIC\,B_{combo}}{MIC\,B_{alone}}$$

where FICI > 1 indicates antagonism, FICI = 1 indicates additivity, and FICI < 1 indicates synergy. The efficacy of the drug combination was also evaluated in the *L. longbeacheae* background, but synergy was not observed.

Data availability. The atomic coordinates and structure factors for Tet(50), Tet(51), Tet(55), Tet(50)–chlortetracycline, Tet(50)–anhydrotetracycline, and Tet(56) have been deposited in the RCSB Protein Data Bank under accession codes: 5TUE, 5TUK, 5TUL, 5TUI, 5TUF, and 5TUM respectively. All other data generated or analyzed during this study are included in this published article (and its Supplementary Information files) or are available from the corresponding author on reasonable request.

50. Merriam, J.J., Mathur, R., Maxfield-Boumil, R. & Isberg, R.R. Analysis of the Legionella pneumophila fliI gene: intracellular growth of a defined mutant defective for flagellum biosynthesis. *Infect. Immun.* **65**, 2497–2501 (1997).
51. Feeley, J.C. *et al.* Charcoal-yeast extract agar: primary isolation medium for Legionella pneumophila. *J. Clin. Microbiol.* **10**, 437–441 (1979).
52. Berger, K.H. & Isberg, R.R. Two distinct defects in intracellular growth complemented by a single genetic locus in Legionella pneumophila. *Mol. Microbiol.* **7**, 7–19 (1993).
53. Sexton, J.A. *et al.* The Legionella pneumophila PilT homologue DotB exhibits ATPase activity that is critical for intracellular growth. *J. Bacteriol.* **186**, 1658–1666 (2004).
54. Kabsch, W. XDS. *Acta Crystallogr. D Biol. Crystallogr.* **66**, 125–132 (2010).
55. Winn, M.D. *et al.* Overview of the CCP4 suite and current developments. *Acta Crystallogr. D Biol. Crystallogr.* **67**, 235–242 (2011).
56. Emsley, P. & Cowtan, K. Coot: model-building tools for molecular graphics. *Acta Crystallogr. D Biol. Crystallogr.* **60**, 2126–2132 (2004).
57. Adams, P.D. *et al.* PHENIX: a comprehensive Python-based system for macromolecular structure solution. *Acta Crystallogr. D Biol. Crystallogr.* **66**, 213–221 (2010).
58. Chen, V.B. *et al.* MolProbity: all-atom structure validation for macromolecular crystallography. *Acta Crystallogr. D Biol. Crystallogr.* **66**, 12–21 (2010).
59. CLSI. *Methods for Dilution Antimicrobial Susceptibility Testing for Bacteria That Grow Aerobically; Approved Standard–Tenth Edition*. Vol. M07–A10 (Clinical and Laboratory Standards Institute, 2015).
60. Berenbaum, M.C. A method for testing for synergy with any number of agents. *J. Infect. Dis.* **137**, 122–130 (1978).